Probing the free energy landscapes of ALS disease mutants of SOD1 by NMR spectroscopy

Ashok Sekhar[a,b,c], Jessica A. O. Rumfeldt[d], Helen R. Broom[d], Colleen M. Doyle[d], Ryan E. Sobering[b], Elizabeth M. Meiering[d], and Lewis E. Kay[a,b,c,e,1]

[a]Department of Molecular Genetics, The University of Toronto, Toronto, ON, Canada M5S 1A8; [b]Department of Biochemistry, The University of Toronto, Toronto, ON, Canada M5S 1A8; [c]Department of Chemistry, The University of Toronto, Toronto, ON, Canada M5S 1A8; [d]Department of Chemistry, University of Waterloo, Waterloo, ON, Canada N2L 3G1; and [e]Program in Molecular Structure and Function, Hospital for Sick Children, Toronto, ON, Canada M5G 1X8

Edited by Gerhard Wagner, Harvard Medical School, Boston, MA, and approved September 23, 2016 (received for review July 12, 2016)

Amyotrophic lateral sclerosis (ALS) is a neurodegenerative disease that, in some cases, has been linked with mutations to the antioxidant metalloenzyme superoxide dismutase (SOD1). Although the mature form of this enzyme is highly stable and resistant to aggregation, the most immature form, lacking metal and a stabilizing intrasubunit disulfide bond, apoSOD1^{2SH}, is dynamic and hypothesized to be a major cause of toxicity in vivo. Previous solution NMR studies of wild-type apoSOD1^{2SH} have shown that the ground state interconverts with a series of sparsely populated and transiently formed conformers, some of which have aberrant nonnative structures. Here, we study seven disease mutants of apoSOD1^{2SH} and characterize their free energy landscapes as a first step in understanding the initial stages of disease progression and, more generally, to evaluate the plasticity of low-lying protein conformational states. The mutations lead to little change in the structures and dynamics of the ground states of the mutant proteins. By contrast, the numbers of low-lying excited states that are accessible to each of the disease mutants can vary significantly, with additional conformers accessed in some cases. Our study suggests that the diversity of these structures can provide alternate interaction motifs for different mutants, establishing additional pathways for new and often aberrant intra- and intermolecular contacts. Further, it emphasizes the potential importance of conformationally excited states in directing both folding and misfolding processes.

superoxide dismutase | free energy landscape | CPMG NMR | CEST NMR | conformationally excited states

Human Cu,Zn superoxide dismutase (SOD1), an extensively studied dimeric metalloenzyme, has served as a prototype for understanding the protein structure-function paradigm and for elucidating how folding and misfolding can be associated with disease (1). In 1993, a genetic link was established between amyotrophic lateral sclerosis (ALS) and mutant forms of SOD1 (2), and currently, over 150 disease-causing mutations have been identified (alsod.iop.kcl.ac.uk/). A characteristic feature of ALS is the presence of protein aggregates in motor neurons (3), of which SOD1 has been identified as a component in some familial ALS (fALS), as well as in some sporadic ALS (sALS) cases (4–6). Due to similarities in the clinical symptoms of fALS and sALS, common aggregation mechanisms have been proposed for both forms of the disease (7, 8). A major hypothesis is that mutations promote misfolding and aggregation of SOD1, leading to a cascade of toxic events that culminate in motor neuron death (9). However, attempts to identify relationships between the diverse set of mutants and disease characteristics, such as age of onset, severity and aggregate morphology, have proven difficult (10, 11).

The fully mature form of SOD1 ($Cu_2Zn_2SOD1^{S\text{-}S}$) is a highly stable homodimer (Fig. 1*A*) with a melting temperature of 92 °C (12) that maintains enzymatic activity even under strongly denaturing conditions (13). Each SOD1 chain adopts an eight-stranded Greek key β-barrel structure with two long loops that are referred to as the zinc-binding (or dimer) loop and the electrostatic loop (1). Zinc and copper binding (one of each metal per monomer), disulfide bond formation, and dimerization limit the flexibility of the loops and markedly increase protein stability (14). Residues in both loops participate in a multitude of hydrogen-bonding interactions that are believed to stabilize the protein by providing a network of connections between the loops and the metal-binding sites (15). Relative to mature SOD1, ALS-associated mutant forms have increased tendencies to be metal-deficient (1), and the loss of metal decreases stability and increases the range of sampled conformations, leading to increased aggregation propensities.

The focus of this study is on the most immature form of SOD1, apoSOD1^{2SH}, which is metal-free, disulfide-reduced, and mainly monomeric under physiological conditions (16). In the absence of metals and disulfide bonds, vital interactions are lost, causing the electrostatic and zinc-binding loops to unravel (17). Together with the exposed dimer interface, loop unraveling leads to an increased tendency of the protein to misfold and establish nonnative contacts. ApoSOD1^{2SH} is highly dynamic, and its stability is relatively low compared with other globular proteins (10), and far lower than more mature forms of SOD1. We have previously shown that apoSOD1^{2SH} populates at least four distinct low-energy, yet thermally accessible, conformational states (referred to here as excited states), with lifetimes on the millisecond time scale (18). Two of these rare conformers are generated by transitions from apoSOD1^{2SH} that lead to the formation of structural elements resembling the structural elements found in $Cu_2Zn_2SOD1^{S\text{-}S}$, whereas the other two conformers are nonnative dimers that are stabilized by aberrant intermolecular interactions (18).

Because apoSOD1^{2SH} is the least stable form of the protein, its free energy landscape would be expected to be perturbed by

Significance

A series of amyotrophic lateral sclerosis disease-causing mutants of superoxide dismutase have been studied using NMR experiments probing sparsely populated, transiently formed protein conformers. Focusing on the most immature enzyme form, which is monomeric, metal-free, and lacking a stabilizing disulfide bond, we show that the ground states for the wild-type and disease mutant proteins are similar, with an intact eight-stranded β-barrel structure resembling the structure of the mature enzyme. In contrast, conformationally excited states can be affected by mutation, both in terms of the number and types of structures accessible to the mutant. These excited states can play roles in both maturation and aggregation processes and, in the latter case, can provide a variety of possible pathways for aberrant interactions.

Author contributions: A.S., E.M.M., and L.E.K. designed research; A.S. and L.E.K. performed research; J.A.O.R., H.R.B., C.M.D., R.E.S., and E.M.M. contributed new reagents/analytic tools; A.S., E.M.M., and L.E.K. analyzed data; A.S., E.M.M., and L.E.K. wrote the manuscript.

The authors declare no conflict of interest.

This article is a PNAS Direct Submission.

[1]To whom correspondence should be addressed. Email: kay@pound.med.utoronto.ca.

This article contains supporting information online at www.pnas.org/lookup/suppl/doi:10.1073/pnas.1611418113/-/DCSupplemental.

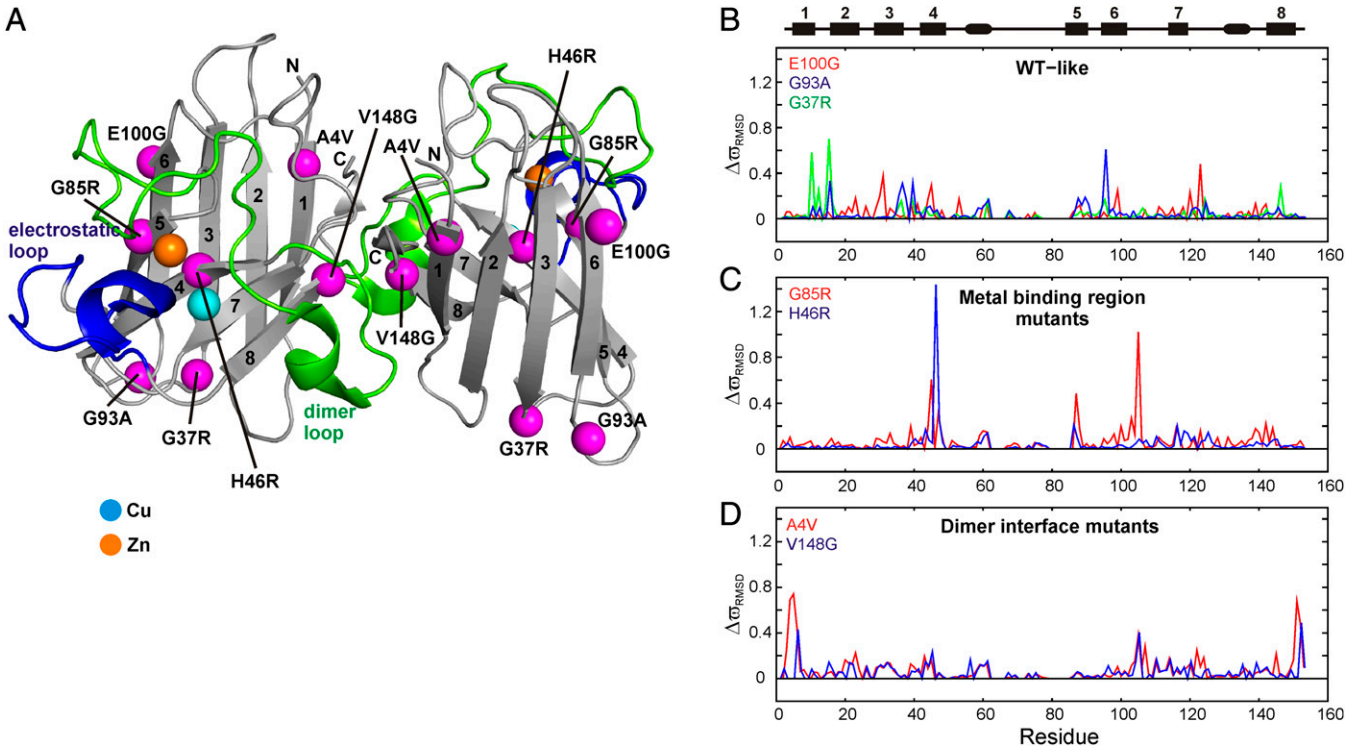

Fig. 1. Disease mutations result in little change to the ground state apoSOD1^{2SH} structure. (*A*) Structure of the mature form of SOD1, $Cu_2Zn_2SOD1^{S\text{-}S}$ [Protein Data Bank ID code 1HL5 (52)] with positions of WT-like, dimer interface, and metal-binding mutations indicated by magenta spheres. The dimer and electrostatic loops are shown in green and blue, respectively. The β-strands are numbered, and Cu and Zn metal ions are denoted by cyan and orange spheres, respectively. Residue-specific differences in ^{15}N and $^{1}H^{N}$ chemical shifts between pWT and mutant apoSOD1^{2SH} are shown for WT-like (*B*), metal-binding region (*C*), and dimer interface (*D*) mutants, quantified as described in the main text. The secondary structure of SOD1 is indicated above *B*, with rectangles and ovals denoting strands and helices, respectively.

disease-causing mutants more readily than the more mature forms of the protein (10). Thus, apoSOD1^{2SH} presents an interesting model for understanding the effects of mutations on free energy landscapes and the plasticity of low-lying protein conformational states. Although many studies have focused on how mutations can lead to structural changes in the ground state of a protein, little is known about how the structural properties of sparsely populated and transiently formed states are affected. Here, we characterize such excited states in seven mutants of SOD1 associated with ALS. Although the mutations cause only minimal perturbations to the native state structure of apoSOD1^{2SH}, they substantially affect the free energy landscape and alter the number, nature, and stability of the thermally accessible rare conformers. The effects of the mutations are both local and long-range, suggesting allosteric pathways of communication within the protein. Intriguingly, two of the mutants have conformational fluctuations in the β_5-β_6 plug region that are not present in wild-type (WT) SOD1, highlighting this region as a "hotspot" for the formation of alternate conformers in addition to the Zn-binding and electrostatic loops.

Results

Mutants Chosen in This Work. As described in the Introduction, we have chosen to study a series of seven ALS-causing mutants in the context of the most immature form of SOD1, apoSOD1^{2SH}. All of the mutations were inserted into a well-established pseudo-WT version of the protein, referred to as pWT, in which surface-exposed and nonconserved Cys-6 and Cys-111 have been replaced by Ala and Ser, respectively (19). These substitutions avoid complications that could arise from disulfide bond formation. pWT SOD1 has been extensively characterized in the literature and retains WT-like structure, folding, and enzymatic activity (1, 10, 15, 20), and cell culture and mouse model studies have found that a disulfide cross-link at these positions is not required for aggregate formation (21) and does not influence the nature of the aggregate structures formed (22). The seven disease mutations are distributed throughout the structure of SOD1 (Fig. 1*A*) and can broadly be classified into three categories based on their location and biophysical properties (1). For simplicity, in what follows, we will refer to the mutant proteins by the mutation itself (i.e., A4V refers to the protein with the A4V mutation). A4V and V148G are proteins with mutations occurring at the native dimer interface, leading to a lower propensity for dimerization than WT SOD1. H46R and G85R are metal-binding region mutants with weaker affinities for metal ions (Zn in the case of G85R and Cu and Zn for H46R), whereas G37R, G93A, and E100G are WT-like in enzymatic activity and metal affinity (1). There is a significant variability in the disease duration (time between age of disease onset and age of death) of patients carrying these mutations, ranging from greater than 17 y for G37R and H46R to ∼5 y for E100G, 1–3 y for G93A, and less than 1 y for A4V (1). A wide range of $\Delta G^{0}_{unfolding}$ values, from 2.5 kcal/mol to −0.2 kcal/mol, has been estimated for these mutants based on quantification of cross-peak intensity ratios in ^{15}N-^{1}H transverse relaxation optimized spectroscopy (TROSY) (23) heteronuclear single quantum coherence (HSQC) spectra, focusing on Trp32 side-chain indole peaks derived from folded and unfolded conformers (Fig. S1 and Table S1), broadly consistent with relative stabilities measured by differential scanning calorimetry (10).

Ground State Structure. Given the diverse nature of the mutations and the broad range of protein stabilities, we first examined the structural perturbations to the ground states introduced by the amino acid replacements. The chemical shift differences between corresponding cross-peaks in ^{15}N-^{1}H TROSY-HSQC spectra of pWT and mutant forms of apoSOD1^{2SH} are very small (Fig. S1)

and are predominantly localized to the site of the mutation (Fig. 1 *B–D*). Only nine of the 939 assigned residues (out of a total of 1,036, taking into account all seven mutants) have $\Delta\varpi_{RMSD}$ values greater than 0.5, where $\Delta\varpi_{RMSD} = \sqrt{\frac{1}{2}\sum_i \left(\frac{\Delta\varpi_i}{\Delta\varpi_{STD,i}}\right)^2}$ (24), $i\ \varepsilon\ (^1H^N, ^{15}N)$, $\Delta\varpi_i$ is the difference in corresponding chemical shifts (parts per million) in spectra of pWT and mutant proteins, and $\Delta\varpi_{STD,i}$ is 1 SD of the chemical shift distribution (both nucleus- and residue-specific) as tabulated in the Biological Magnetic Resonance Bank (www.bmrb.wisc.edu). Of these nine residues, only five are further than 5 aa from the site of mutation. The chemical shift data establish that all of the mutant forms of apoSOD1^{2SH} examined here are structurally similar to pWT and have an intact β-barrel. In addition, they are consistent with dynamic dimer and electrostatic loops, because low chemical shift-derived order parameters were calculated previously for pWT apoSOD1^{2SH} in these regions (18) and amide ^{1}H and ^{15}N nuclei for loop residues resonate in near-identical positions in all apoSOD1^{2SH} variants. Notably, large amide shift differences are observed between apoSOD1^{2SH} and Cu_2Zn_2SOD1$^{S\text{-}S}$ (by as much as 9 ppm in ^{15}N) especially in the dimer/electrostatic loop regions of the protein, where these loops have become well-structured in the mature enzyme (18).

Thermally Accessible Conformations in Mutant apoSOD1^{2SH}. In a previous study, we have detected and structurally characterized four thermally accessible excited state conformers for pWT apoSOD1^{2SH} that are in equilibrium with the ground state (18). To investigate the conformational free energy landscapes of the seven mutants of apoSOD1^{2SH}, focusing to a large extent on the excited states that have been characterized previously, we performed a series of ^{15}N chemical exchange saturation transfer (CEST) (25, 26) and ^{15}N Carr–Purcell–Meiboom–Gill (CPMG) (27, 28) relaxation dispersion experiments. The underlying mechanisms of both of these experiments have been described in detail previously (26, 29–32). Briefly, in CEST-based experiments, the effect of a weak radiofrequency perturbation (typically 10–50 Hz), applied at the frequency of an "invisible" resonance of the excited state conformer, is transferred via chemical exchange to the corresponding resonance in the ground state. This transfer leads to an effective amplification of the "signals" from the rare conformer, as observed through the ground conformer. For a two-state exchange process, a CEST profile is obtained for each amide, which is composed of dips at the positions of the ground (large dip) and excited (small dip) state chemical shifts, whereas only the ground state dip is observed in the absence of exchange. The CPMG experiment exploits the increase in effective transverse relaxation rates of NMR spins ($R_{2,eff}$) due to millisecond time-scale stochastic fluctuations between protein states. The application of chemical shift refocusing pulses can modulate $R_{2,eff}$, giving rise to dispersion profiles that quantify $R_{2,eff}$ as a function of the rate of application of the pulses (ν_{CPMG}). Large dispersion profiles, corresponding to substantial differences in $R_{2,eff}$ at low and high pulsing frequencies, are hallmarks of millisecond time-scale exchange, whereas flat profiles indicate the absence of such processes. Both classes of experiments have been shown to be particularly powerful, in concert, to dissect the complicated "exchange landscape" that is present in pWT apoSOD1^{2SH} (18). Here, we use the presence of small dips in CEST profiles and nonflat relaxation dispersion profiles as a "screen" to establish qualitatively whether exchange processes are present, and hence to explore the free energy landscapes of ALS disease mutants. It is important to emphasize that each of these relaxation approaches is restricted in terms of the time scales of exchange events that can be quantified, limiting to some extent the regions of the landscape that are accessible. The CEST experiment is sensitive to exchange processes that range from ∼50 to 500 s^{-1}, whereas the CPMG approach quantifies interconversion rates on the order of 100 to 3,000 s^{-1} (33). Thus, despite the fact that peaks corresponding to the unfolded state of apoSOD1^{2SH} are present in spectra of some of the disease mutants studied, the folding/unfolding of the protein cannot be explored using CEST or CPMG experiments because the folding rate constant of apoSOD1^{2SH}, 0.023 s^{-1} at 25 °C and pH 6.3 (34), is well outside the detection window of these methods.

In what follows, we initially focus on each of the four exchange processes previously detected in pWT apoSOD1^{2SH} (18) and establish whether they are present in the seven disease mutants considered here. Process I corresponds to the interconversion between monomeric (ground state) apoSOD1^{2SH} and a dimeric form of the protein (excited state) that structurally resembles Cu_2Zn_2SOD1$^{S\text{-}S}$. The exchange event is illustrated in Fig. 2*A* (*Top*), along with the lifetime (τ) and population (p_E) of the excited state conformer that was established previously for pWT apoSOD1^{2SH} (25 °C) (18). As described in that study, Gly-61 is a reporter of process I and the ^{15}N CEST profile for this residue shows a minor dip at ∼100 ppm that derives from the dimeric excited state (Fig. 2*B*). We have used this profile, along with others from residues Gly-51, Asn-53, and Thr-54, to establish whether this dimer-forming process is present in each of the disease mutants studied. All WT-like and metal-binding region mutants retain this excited state, because CEST profiles for these residues clearly show a second dip at the position expected for the dimer (Fig. S2). However, for the two dimer interface mutants studied here, the second dip is barely observed (A4V) or notably absent (V148G) (Fig. 2*C*), indicating that the population of the dimer must be at or below the detection threshold of the experiment, typically less than 0.3% for the exchange parameters relevant for process I (Fig. 2*A*).

A second exchange event (process II) that also involves formation of native-like structure has been characterized for pWT apoSOD1^{2SH} (18). Here, a short helix in the electrostatic loop (Fig. 1*A*) that is not present in the ground state of apoSOD1^{2SH} is formed in the excited conformer (Fig. 2*D*). Residues Thr-135 and Thr-137 of the electrostatic loop are reporters of this process and undergo large ($\Delta\varpi \sim 9$ ppm) chemical shift changes that can be readily observed in ^{15}N CEST profiles of pWT apoSOD1^{2SH} (Fig. 2*E*). Minor dips for both Thr-135 and Thr-137 are observed for WT-like mutants G93A and G37R (Fig. 2*F*) but are absent or severely attenuated for the metal-binding region mutants H46R and G85R and for the dimer interface and WT-like mutants V148G and E100G, respectively. This finding indicates that the helix does not form or forms at a level that is at the threshold of detection in these variants (Fig. 2 *F–H*).

A pair of additional conformational exchange processes, resulting in the formation of nonnative apoSOD1^{2SH} dimers, has also been characterized (18) (Fig. 3 *A* and *D*). One of these exchange processes, the dimer formed via process III, is symmetrical and involves the native dimer interface, whereas the other (formed via process IV) is asymmetrical and is stabilized through interactions of the electrostatic loop of one monomer with the native dimer interface of another. Both of these exchange processes involve relatively smaller chemical shift differences in comparison to transitions I and II described above, and CPMG relaxation dispersion experiments have proven critical for their study. Residues such as Gly-114 and Gln-153 (process III; Fig. 3 *B* and *C*) as well as Ser-111 and His-46 (process IV; Fig. 3 *E* and *F*), among others, serve as reporters. As illustrated in Fig. S3, most of the mutant apoSOD1^{2SH} variants retain the ability to form nonnative dimers. Structural models of these nonnative dimers predict that mutations weakening the native dimer interface would disrupt formation of the excited state nonnative dimers (discussed below). This disruption is observed for both of the dimer-disrupting mutants considered in this study, A4V and V148G, where flat or very significantly reduced dispersion profiles (Fig. 3 *C* and *F*) relative to the dispersion profiles for the pWT protein (Fig. 3 *B* and *E*) are recorded, indicating a significant reduction in the populations of both aberrant dimeric states (processes III and IV).

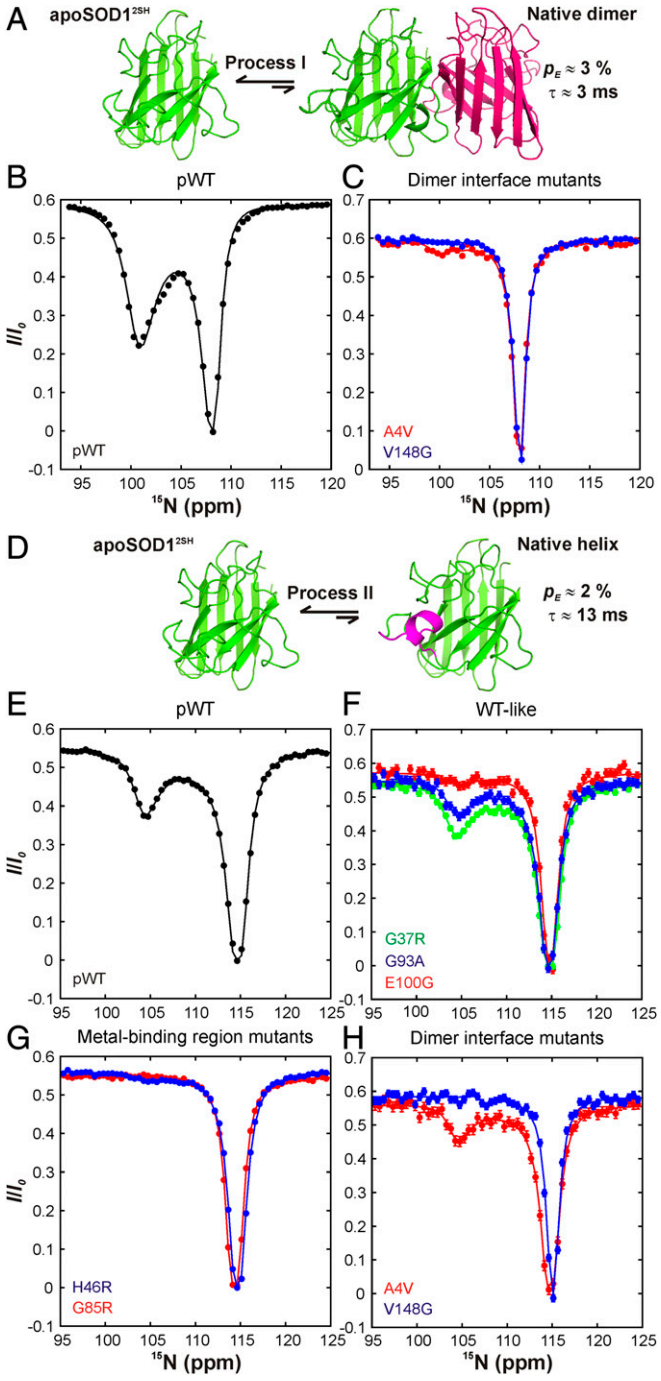

Fig. 2. Effect of disease mutations on excited states of apoSOD1^{2SH} generated via processes I and II. (*A*) Schematic of the transient dimerization (process I) of apoSOD1^{2SH}, with the population (p_E) and lifetime (τ) of the dimeric state indicated for pWT apoSOD1^{2SH} [25 °C, 1.3 mM apoSOD1^{2SH} (18)]. ^{15}N CEST profiles for Gly-61 reporting on native dimerization for pWT (*B*) and dimer interface (*C*) mutants are shown. Note that profiles for Gly-61 are representative of the profiles for other residues probing process I, such as Gly-51, Asn-53, and Thr-54. (*D*) Schematic as in *A*, but for process II in which a native helix is transiently formed in the electrostatic loop. ^{15}N CEST profiles of Thr-135 reporting on helix formation for pWT (*E*), WT-like (*F*), metal-binding region (*G*), and dimer interface (*H*) mutants are shown. Solid lines are best fits of residue- and B_1-specific CEST profiles to a two-state model of chemical exchange.

Our results establish that not all of the four excited states previously characterized for pWT apoSOD1^{2SH} are observed for each of the ALS disease mutants. However, this fact does not imply that they have simpler free energy landscapes. For example, additional rare conformers are accessible for G85R and G93A that are notably absent in the pWT protein (Fig. 4). CPMG (G85R; Fig. 4*A*) and CPMG/CEST (G93A; Fig. 4 *C* and *D*) analyses indicate conformational fluctuations in the β_5-β_6 cleft that involve a large number of residues (Fig. 4 *B* and *E*). Interestingly, despite the fact that the exchange is localized to the same region of structure (β_5-β_6) for both G85R and G93A, the exchange dynamics are somewhat different for each mutant. The exchange rate for G85R is fast on the chemical shift time scale, as evidenced by the near-linear decrease in $R_{2,eff}$ with ν_{CPMG} (exchange rate > 3,000 s^{-1}, 25 °C, based on global fits of profiles from all reporter residues to a two-state

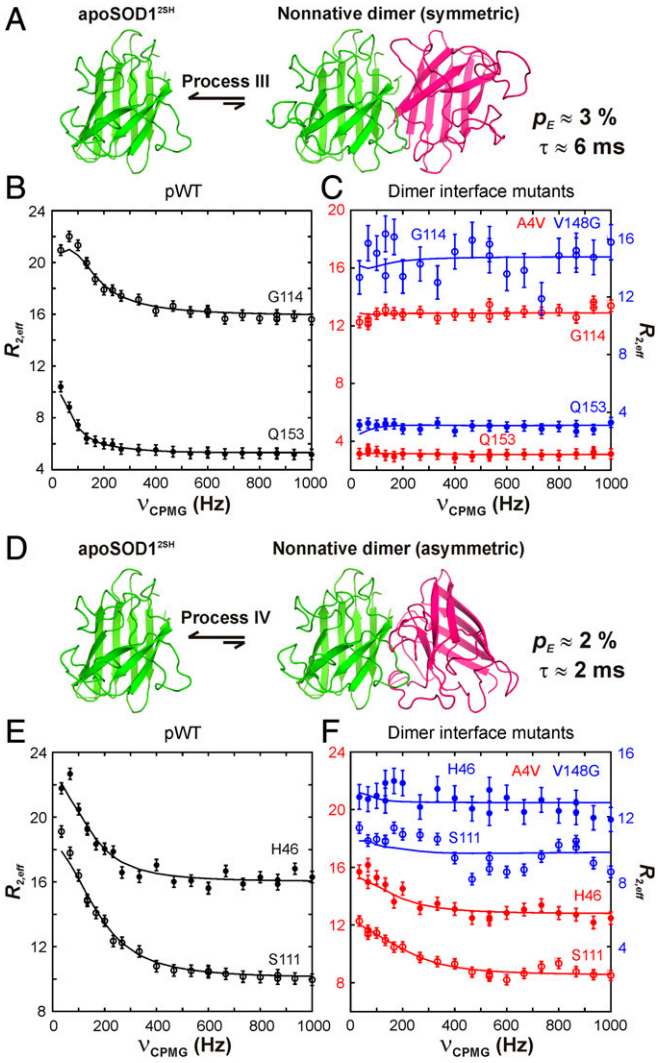

Fig. 3. Effect of disease mutations on aberrant dimeric excited states of apoSOD1^{2SH} generated via processes III and IV. (*A*) Schematic of the exchange process generating the symmetrical dimer excited state, process III, with p_E and τ indicated [25 °C, 1.3 mM apoSOD1^{2SH} (18)]. ^{15}N CPMG profiles for Gly-114 (○) and Gln-153 (●) reporting on symmetrical nonnative dimerization for pWT (*B*) and dimer interface (*C*) mutants are shown. (*D*) Schematic as in *A*, but for process IV. ^{15}N CPMG profiles for Ser-111 (○) and His-46 (●) reporting on asymmetrical nonnative dimerization for pWT (*E*) and dimer interface (*F*) mutants are shown. Solid lines are global fits of CPMG profiles obtained at 14.1 T and 18.8 T. In *C* and *F*, *y* axes for A4V and V148G are offset so that dispersions are not overlapping. Note that the exchange processes relevant in *A* and *D* are depicted using cartoon representations of the structural models obtained previously both for pWT apoSOD1^{2SH} and for the symmetrical and asymmetrical nonnative dimers (18).

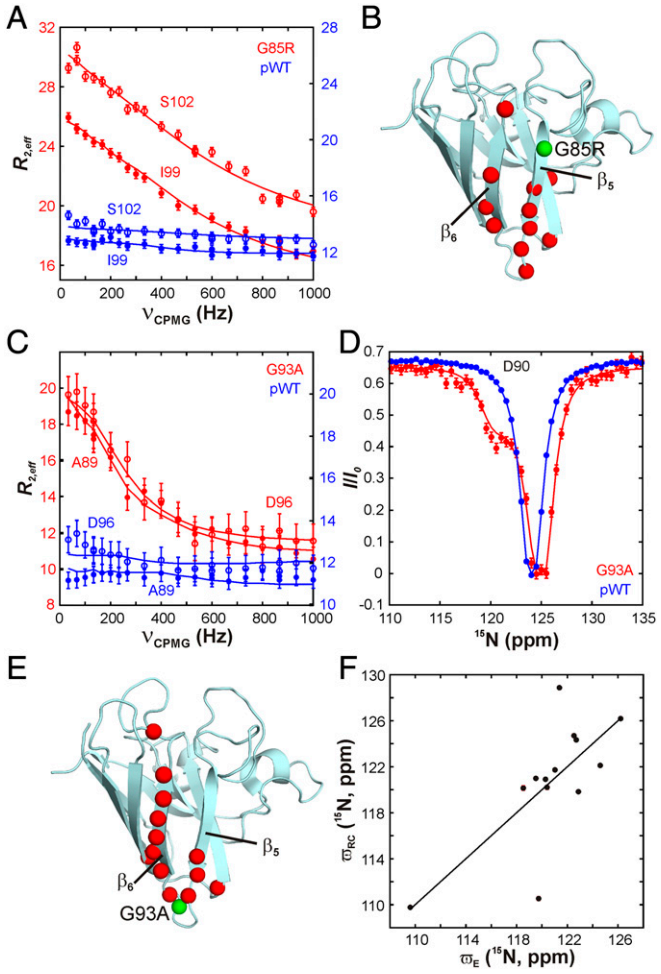

Fig. 4. Additional conformational exchange processes for G85R and G93A implicate the β_5-β_6 cleft as a dynamic hotspot. (*A*) CPMG relaxation dispersion profiles for Ile-99 (●) and Ser-102 (○) of G85R (red) and pWT (blue) apoSOD1^{2SH}. (*B*) Residues reporting on this exchange process that could be globally fit to a two-state model of exchange are plotted as red spheres on the monomer structure of SOD1. The location of G85 is indicated by a green sphere. (*C*) ^{15}N CPMG profiles for Ala-89 (●) and Asp-96 (○) of G93A (red) and pWT (blue) constructs. (*D*) ^{15}N CEST profile for Asp-90 of G93A (red) and pWT (blue). (*E*) Residues reporting on this exchange process that could be globally fit to a two-state model of exchange are plotted as red spheres on the monomer structure of SOD1, with the location of G93 indicated by a green sphere. (*F*) Chemical shifts of the excited state populated by G93A obtained from a global analysis of CEST and CPMG relaxation data correlate well, but not perfectly, with random coil values [as tabulated by Tamiola et al. (53)], suggesting that the excited conformation is less structured than the native state.

model), and in this exchange regime, it is not possible to extract chemical shifts for nuclei in the excited state from CPMG profiles alone. For G93A, the exchange time scale was reduced so that a combined CPMG/CEST analysis could be performed. Exchange parameters $p_E = 1.60 \pm 0.05\%$ and $\tau = 1.40 \pm 0.03$ ms, 25 °C, were fit along with chemical shifts of the excited state that correlate broadly, but not perfectly, with random coil chemical shifts (Fig. 4*F*). This correlation strongly indicates that the β_5-β_6 cleft opens and becomes partially unstructured in apoSOD1^{2SH} G93A, as was also suggested in a previous study of the holo form of G93A (35).

Discussion

In this study, we have used both CEST and CPMG NMR spin relaxation methods to detect sparsely populated conformational states in disease mutants of the most immature form of human superoxide dismutase 1 (apoSOD1^{2SH}), which lacks metal ions and a stabilizing intramonomer disulfide bond. Unlike the mature form of this antioxidant enzyme, which is highly stable, apoSOD1^{2SH} misfolds and aggregates in vitro (14, 36, 37), and may be a primary cause of toxicity in vivo (38). Thus, it is of considerable interest to characterize the free energy landscape of both WT and disease mutant forms of the protein as a first step toward understanding the initial stages of disease progression. Our results establish that the conformational free energy landscapes of both WT apoSOD1^{2SH} and many of the disease mutants of this immature form contain a number of low-lying excited conformers, with as many as five detected in the present analysis for G93A (although process III is highly attenuated for this mutant). Regions of conformational heterogeneity and a list of the sparse conformers detected for pWT and each of the disease mutants are presented in Fig. 5. The detected excited states are structurally distinct from the native state conformer or the globally unfolded state, and thus provide alternate interaction motifs and new pathways for the establishment of aberrant intra- and intermolecular contacts.

Analysis of the CPMG and CEST relaxation profiles of reporter residues in each of the seven disease-causing mutants that have been chosen for study here (A4V, G37R, H46R, G85R, G93A, E100G, and V148G) clearly shows that the mutations can differentially affect the apoSOD1^{2SH} free energy landscape, with the numbers of observed excited states varying from zero (V148G) to possibly five (G93A) (Fig. 5*B*). This variability is a feature that cannot be predicted from traditional structural biology studies that focus only on the ground state, because the ground state conformers of all disease mutants share the same eight-stranded, β-barrel structure and dynamic Zn-binding and electrostatic loops (Fig. 1 and Fig. S1). Further, the facile accessibility of pWT apoSOD1^{2SH} and a number of the ALS disease mutants to alternative, rare-state conformations implies that an understanding of the aberrant interactions of SOD1 with in vivo binding partners cannot be achieved purely on the basis of the ground state structure. Rather, a comprehensive knowledge of the thermally accessible alternate conformations that can play important roles in forming these interactions is required. It is tempting to speculate that the observed variability in excited state structural propensities may partly be responsible for the heterogeneous nature of ALS and for the disparity in disease onset, pathology, survival time, and aggregate morphology, because each disease-causing mutant can have its own set of accessible conformers from which to form potentially different aberrant structures. Indeed, it has been hypothesized on the basis of computational studies that differences in dynamics between diverse disease-causing mutants can result in varied patterns of local folding, which, in turn, may affect aggregate morphology (39). Our results are consistent with this idea, revealing distinct free energy landscapes for the different SOD1 mutants. A case in point is provided by G85R and G93A, where the β_5-β_6 cleft becomes destabilized in one of the several excited states that is accessible to each of these mutant proteins (Fig. 4). This destabilization results in partial unfolding of the β_5-β_6 region, at least for G93A (Fig. 4*F*), and, potentially, the formation of conformers that lead to nonnative oligomers. Support for this aggregation model comes from the crystal structures of S134N Cu_2Zn_2SOD1$^{S\text{-}S}$ and H46R apoSOD1$^{S\text{-}S}$ that show nonnative interfaces between adjacent SOD1 molecules consisting of the β_5-β_6 cleft of one molecule and the electrostatic loop of another (40). Thus, β_5-β_6 can serve as a hotspot for the formation of aggregates that would normally not form if the electrostatic loop is rigidly held in place by a network of hydrogen bonds. Disordering of the electrostatic loop in apoSOD1^{2SH} and further destabilization of the β_5-β_6 cleft in G85R and G93A could provide a pathway to aggregation.

Excited state conformers of apoSOD1^{2SH} may play important roles in the natural maturation process as well. In this context, the absence of a transiently formed, native-like dimer in equilibrium with the monomeric A4V and V148G apoSOD1^{2SH} ground states

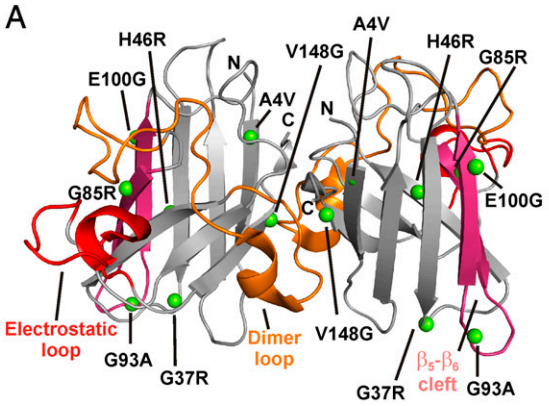

B

Mutation	Process I (native dimer)	Process II (native helix)	Process III (symmetric non-native dimer)	Process IV (asymmetric non-native dimer)	β_5-β_6 cleft dynamics
pWT	+	+	+	+	-
A4V	⊖	+	-	⊖	-
G37R	+	+	+	+	-
H46R	+	⊖	+	+	-
G85R	+	-	+	+	+
G93A	+	+	⊖	+	+
E100G	+	⊖	+	+	-
V148G	-	-	-	-	-

⊖ Indicates that the process is highly attenuated

Fig. 5. Dynamic hotspots in apoSOD1^{2SH} as established by NMR spin relaxation. (*A*) Cartoon representation of the structure of the $Cu_2Zn_2SOD1^{S\text{-}S}$ native dimer, with regions forming sparse conformers in apoSOD1^{2SH} (both pWT and disease-causing mutants) indicated in red (electrostatic loop), orange (dimer loop), and pink (β_5-β_6 cleft). The locations of the mutations studied are depicted by green spheres. (*B*) Mutants studied in this work, listing the presence (+) or absence (–) of conformational exchange processes I–IV observed in pWT, as well as β_5-β_6 cleft dynamics.

(process I; Fig. 2*C*) is particularly interesting, given that measurements show that both A4V and V148G $Cu_2Zn_2SOD1^{S\text{-}S}$ have lower dimerization constants than the WT protein (41). This finding suggests that formation of a dimeric excited state may expedite the generation of a highly stable dimer. However, it is worth noting that A4V and V148G $Cu_2Zn_2SOD1^{S\text{-}S}$ are both predominantly dimeric (42), so that the critical factor in dimer formation is nevertheless posttranslational binding of metal ions and/or disulfide bond formation. Another example illustrating the potential importance of excited states in the SOD1 maturation process, starting from apoSOD1^{2SH}, is provided by the metal-binding mutants H46R and G85R. Here, the absence or severe attenuation of minor state dips in CEST profiles for residues Thr-135 and Thr-137 indicates that the native-like electrostatic loop helix does not form in the excited states of these mutants. The dipole of this short helix has been proposed to stabilize the binding of Zn (43), and its conspicuous absence in mutants with lower Zn affinities may indicate that metal binding is facilitated, at least in part, through a conformational selection mechanism with zinc binding to excited state conformers containing the transiently formed helix in the electrostatic loop. Notably, the helix is at the limit of detection or not present in the excited states of E100G and V148G, respectively, where the sites of mutations are more than 20 Å away from Thr-135. The fact that these distant mutations can affect local folding at the electrostatic loop emphasizes the importance of allosteric pathways in apoSOD1^{2SH}. Finally, there is an interesting parallel between excursions of apoSOD1^{2SH} to the rare, short-lived conformers described above via processes I and II and the transitions that are made by the enzyme dihydrofolate reductase (DHFR) during its reaction cycle, as detailed by Wright and coworkers (44). In both cases, rare conformers are visited from ground states, ultimately becoming dominant conformers as the maturation process (SOD1) or reaction cycle (DHFR) proceeds, with the presampling of subsequent conformations likely playing an important role in directing each process.

Although the SOD1 disease mutations examined here have little impact on the global structural and dynamical properties of the corresponding ground state conformers, substantial differences are noted for the low-lying excited states that are in equilibrium with them. These differences include both the number and the structures of excited conformers that are accessible to a given mutant. In addition to providing insight into how ALS disease-causing mutants affect the free energy landscape of SOD1, this study is among the first to describe how mutations affect the structural and dynamic properties of individual excited states. Since the pioneering development of site-directed mutagenesis four decades ago (45), much has been learned about how mutations affect the dominant conformers of proteins. With the development and routine application of NMR spin relaxation experiments such as CPMG relaxation dispersion and CEST (33, 46), it is now possible to begin to assess how mutations affect other regions of the free energy landscape as well. Given the continuing realization of the importance of conformationally excited states in both protein function and misfunction (33, 44, 47), such assessments will only become increasingly relevant.

Materials and Methods

Sample Preparation. Seven mutants of apoSOD1^{2SH} (in a pWT background where Cys-6 and Cys-111 have been replaced by Ala and Ser, respectively), along with the pWT protein, were overexpressed and purified as described earlier (18). NMR samples of ^{15}N-labeled protein were prepared in 20 mM Hepes (pH 7.4) containing 1 mM NaN_3, 1 mM Tris(2-carboxyethyl)phosphine (TCEP), and 10% (vol/vol) D_2O at the following protein concentrations: pWT, 1.3 mM; E100G, 1.2 mM; G93A, 0.7 mM; G37R, 2.0 mM; G85R, 1.5 mM; H46R, 2.5 mM; A4V, 1.1 mM; and V148G, 0.6 mM. Samples were placed in Suprasil NMR tubes (catalog no. 535-PP-7SUP; Wilmad), which were then purged with Ar and sealed.

NMR Spectroscopy. All NMR spectra were acquired using either a Varian 600 MHz (14.1 T) spectrometer equipped with a cryogenically cooled probe or a Varian 800 MHz (18.8 T) spectrometer with a room temperature probe. Sample temperature was measured using a thermocouple placed inside an NMR tube; all experiments were performed at 25 °C.

Assignment of ^{15}N-^{1}H HSQC Spectra of Mutant apoSOD1^{2SH}. ^{15}N-^{1}H HSQC spectra of mutants of apoSOD1^{2SH} were assigned by transferring assignments from pWT apoSOD1^{2SH} and verifying the assignments by recording 150-ms mixing time ^{15}N-edited NOESY datasets (48).

CEST. All ^{15}N CEST datasets were acquired at 600 MHz using a previously reported pulse sequence (26), an exchange duration of 350 ms, and weak B_1 fields of 30 and 58 Hz, calibrated as described earlier (26) (the exact values of B_1 fields vary by ±1 Hz depending on the experiment). Pseudo-3D datasets comprising 89 ($B_1 = 30$ Hz) and 50 ($B_1 = 58$ Hz) planes were collected, corresponding to total acquisition times of 50 h and 30 h, respectively, with the frequency of the weak B_1 field ranging between 93 and 132 ppm.

CPMG. ^{15}N CPMG datasets were acquired at static magnetic fields of 14.1 T and 18.8 T using a previously reported pulse scheme (28) and a constant-time CPMG element of 30 ms. Approximately 20 ν_{CPMG} values were used for each dispersion profile, ranging from 33.3 to 1,000 Hz, with two to three points repeated for error analysis, giving rise to net acquisition times of ~17 h for each pseudo-3D experiment.

Data Analysis. NMR datasets were processed with nmrPipe (49) and visualized using nmrDraw (49) and Sparky (50). Resonance intensities were quantified as a function of the frequency of the weak B_1 field in CEST experiments or the frequency of application of 180° pulses in CPMG experiments using the program FuDA, whereby peak line shapes were fit globally across all frequency values. CEST profiles, I/I_o vs. B_1 field position, were constructed from peak intensities recorded with (I) and without (I_o) the relaxation interval, T_{relax}. CPMG profiles, $R_{2,eff} = -1/T_{relax}\ln(I/I_o)$ vs. ν_{CPMG}, were generated from measured I and I_o values corresponding to peak intensities with (I) and without (I_o) the CPMG relaxation element of duration T_{relax}. CEST and CPMG profiles were fit to a two-site chemical exchange model (51) using the software packages Chemex (https://github.com/gbouvignies/chemex) and CPMG, Anti-TROSY, and TROSY Intelligent Analysis (CATIA), respectively.

ACKNOWLEDGMENTS. This work was supported by Grant MOP-106689 (to E.M.M.) and Grant 257695 (to L.E.K.) from the Canadian Institutes of Health Research and by Natural Sciences and Engineering Research Council Grants RGPIN-184036-2011 and RGPIN-2016-05733 (to E.M.M.). L.E.K. holds a Canada Research Chair in Biochemistry.

1. Valentine JS, Doucette PA, Zittin Potter S (2005) Copper-zinc superoxide dismutase and amyotrophic lateral sclerosis. *Annu Rev Biochem* 74:563–593.
2. Deng H-X, et al. (1993) Amyotrophic lateral sclerosis and structural defects in Cu,Zn superoxide dismutase. *Science* 261(5124):1047–1051.
3. Strong MJ, Kesavapany S, Pant HC (2005) The pathobiology of amyotrophic lateral sclerosis: A proteinopathy? *J Neuropathol Exp Neurol* 64(8):649–664.
4. Okamoto Y, et al. (2011) Colocalization of 14-3-3 proteins with SOD1 in Lewy body-like hyaline inclusions in familial amyotrophic lateral sclerosis cases and the animal model. *PLoS One* 6(5):e20427.
5. Kato S, et al. (2000) New consensus research on neuropathological aspects of familial amyotrophic lateral sclerosis with superoxide dismutase 1 (SOD1) gene mutations: Inclusions containing SOD1 in neurons and astrocytes. *Amyotroph Lateral Scler Other Motor Neuron Disord* 1(3):163–184.
6. Matsumoto S, et al. (1996) Sporadic amyotrophic lateral sclerosis with dementia and Cu/Zn superoxide dismutase-positive Lewy body-like inclusions. *Clin Neuropathol* 15(1):41–46.
7. Rotunno MS, Bosco DA (2013) An emerging role for misfolded wild-type SOD1 in sporadic ALS pathogenesis. *Front Cell Neurosci* 7:253.
8. Tandan R, Bradley WG (1985) Amyotrophic lateral sclerosis: Part 1. Clinical features, pathology, and ethical issues in management. *Ann Neurol* 18(3):271–280.
9. Robberecht W, Philips T (2013) The changing scene of amyotrophic lateral sclerosis. *Nat Rev Neurosci* 14(4):248–264.
10. Vassall KA, et al. (2011) Decreased stability and increased formation of soluble aggregates by immature superoxide dismutase do not account for disease severity in ALS. *Proc Natl Acad Sci USA* 108(6):2210–2215.
11. Wang Q, Johnson JL, Agar NY, Agar JN (2008) Protein aggregation and protein instability govern familial amyotrophic lateral sclerosis patient survival. *PLoS Biol* 6(7):e170.
12. Stathopulos PB, et al. (2006) Calorimetric analysis of thermodynamic stability and aggregation for apo and holo amyotrophic lateral sclerosis-associated Gly-93 mutants of superoxide dismutase. *J Biol Chem* 281(10):6184–6193.
13. Lyons TJ, Gralla EB, Valentine JS (1999) Biological chemistry of copper-zinc superoxide dismutase and its link to amyotrophic lateral sclerosis. *Met Ions Biol Syst* 36:125–177.
14. Furukawa Y, O'Halloran TV (2005) Amyotrophic lateral sclerosis mutations have the greatest destabilizing effect on the apo- and reduced form of SOD1, leading to unfolding and oxidative aggregation. *J Biol Chem* 280(17):17266–17274.
15. Parge HE, Hallewell RA, Tainer JA (1992) Atomic structures of wild-type and thermostable mutant recombinant human Cu,Zn superoxide dismutase. *Proc Natl Acad Sci USA* 89(13):6109–6113.
16. Hörnberg A, Logan DT, Marklund SL, Oliveberg M (2007) The coupling between disulphide status, metallation and dimer interface strength in Cu/Zn superoxide dismutase. *J Mol Biol* 365(2):333–342.
17. Antonyuk S, et al. (2005) Structural consequences of the familial amyotrophic lateral sclerosis SOD1 mutant His46Arg. *Protein Sci* 14(5):1201–1213.
18. Sekhar A, et al. (2015) Thermal fluctuations of immature SOD1 lead to separate folding and misfolding pathways. *eLife* 4:e07296.
19. Getzoff ED, et al. (1992) Faster superoxide dismutase mutants designed by enhancing electrostatic guidance. *Nature* 358(6384):347–351.
20. McRee DE, et al. (1990) Changes in crystallographic structure and thermostability of a Cu,Zn superoxide dismutase mutant resulting from the removal of a buried cysteine. *J Biol Chem* 265(24):14234–14241.
21. Karch CM, Prudencio M, Winkler DD, Hart PJ, Borchelt DR (2009) Role of mutant SOD1 disulfide oxidation and aggregation in the pathogenesis of familial ALS. *Proc Natl Acad Sci USA* 106(19):7774–7779.
22. Karch CM, Borchelt DR (2008) A limited role for disulfide cross-linking in the aggregation of mutant SOD1 linked to familial amyotrophic lateral sclerosis. *J Biol Chem* 283(20):13528–13537.
23. Pervushin K, Riek R, Wider G, Wüthrich K (1997) Attenuated T2 relaxation by mutual cancellation of dipole-dipole coupling and chemical shift anisotropy indicates an avenue to NMR structures of very large biological macromolecules in solution. *Proc Natl Acad Sci USA* 94(23):12366–12371.
24. Bouvignies G, et al. (2011) Solution structure of a minor and transiently formed state of a T4 lysozyme mutant. *Nature* 477(7362):111–114.
25. Fawzi NL, Ying J, Ghirlando R, Torchia DA, Clore GM (2011) Atomic-resolution dynamics on the surface of amyloid-β protofibrils probed by solution NMR. *Nature* 480(7376):268–272.
26. Vallurupalli P, Bouvignies G, Kay LE (2012) Studying "invisible" excited protein states in slow exchange with a major state conformation. *J Am Chem Soc* 134(19):8148–8161.
27. Palmer AG, 3rd, Kroenke CD, Loria JP (2001) Nuclear magnetic resonance methods for quantifying microsecond-to-millisecond motions in biological macromolecules. *Methods Enzymol* 339:204–238.
28. Vallurupalli P, Hansen DF, Stollar E, Meirovitch E, Kay LE (2007) Measurement of bond vector orientations in invisible excited states of proteins. *Proc Natl Acad Sci USA* 104(47):18473–18477.
29. Forsén S, Hoffman RA (1963) Study of moderately rapid chemical exchange reactions by means of nuclear magnetic double resonance. *J Chem Phys* 39(11):2892–2901.
30. Lauzon CB, van Zijl P, Stivers JT (2011) Using the water signal to detect invisible exchanging protons in the catalytic triad of a serine protease. *J Biomol NMR* 50(4):299–314.
31. Carr HY, Purcell EM (1954) Effects of diffusion on free precession in nuclear magnetic resonance experiments. *Phys Rev* 94(3):630–638.
32. Meiboom S, Gill D (1958) Modified spin-echo method for measuring nuclear relaxation times. *Rev Sci Instrum* 29(8):688–691.
33. Sekhar A, Kay LE (2013) NMR paves the way for atomic level descriptions of sparsely populated, transiently formed biomolecular conformers. *Proc Natl Acad Sci USA* 110(32):12867–12874.
34. Lindberg MJ, Normark J, Holmgren A, Oliveberg M (2004) Folding of human superoxide dismutase: Disulfide reduction prevents dimerization and produces marginally stable monomers. *Proc Natl Acad Sci USA* 101(45):15893–15898.
35. Doyle CM, et al. (2016) Concurrent increases and decreases in local stability and conformational heterogeneity in Cu, Zn superoxide dismutase variants revealed by temperature-dependence of amide chemical shifts. *Biochemistry* 55(9):1346–1361.
36. Sheng Y, Chattopadhyay M, Whitelegge J, Valentine JS (2012) SOD1 aggregation and ALS: Role of metallation states and disulfide status. *Curr Top Med Chem* 12(22):2560–2572.
37. Broom HR, Rumfeldt JA, Meiering EM (2014) Many roads lead to Rome? Multiple modes of Cu,Zn superoxide dismutase destabilization, misfolding and aggregation in amyotrophic lateral sclerosis. *Essays Biochem* 56(1):149–165.
38. Zetterström P, Graffmo KS, Andersen PM, Brännström T, Marklund SL (2013) Composition of soluble misfolded superoxide dismutase-1 in murine models of amyotrophic lateral sclerosis. *Neuromolecular Med* 15(1):147–158.
39. Khare SD, Wilcox KC, Gong P, Dokholyan NV (2005) Sequence and structural determinants of Cu, Zn superoxide dismutase aggregation. *Proteins* 61(3):617–632.
40. Elam JS, et al. (2003) Amyloid-like filaments and water-filled nanotubes formed by SOD1 mutant proteins linked to familial ALS. *Nat Struct Biol* 10(6):461–467.
41. Broom HR, Rumfeldt JA, Vassall KA, Meiering EM (2015) Destabilization of the dimer interface is a common consequence of diverse ALS-associated mutations in metal free SOD1. *Protein Sci* 24(12):2081–2089.
42. Broom HR, et al. (2016) Combined isothermal titration and differential scanning calorimetry define three-state thermodynamics of fALS-associated mutant Apo SOD1 dimers and an increased population of folded monomer. *Biochemistry* 55(3):519–533.
43. Cao X, et al. (2008) Structures of the G85R variant of SOD1 in familial amyotrophic lateral sclerosis. *J Biol Chem* 283(23):16169–16177.
44. Boehr DD, McElheny D, Dyson HJ, Wright PE (2006) The dynamic energy landscape of dihydrofolate reductase catalysis. *Science* 313(5793):1638–1642.
45. Hutchison CA, 3rd, et al. (1978) Mutagenesis at a specific position in a DNA sequence. *J Biol Chem* 253(18):6551–6560.
46. Anthis NJ, Clore GM (2015) Visualizing transient dark states by NMR spectroscopy. *Q Rev Biophys* 48(1):35–116.
47. Tzeng S-R, Kalodimos CG (2013) Allosteric inhibition through suppression of transient conformational states. *Nat Chem Biol* 9(7):462–465.
48. Zhang O, Kay LE, Olivier JP, Forman-Kay JD (1994) Backbone 1H and 15N resonance assignments of the N-terminal SH3 domain of drk in folded and unfolded states using enhanced-sensitivity pulsed field gradient NMR techniques. *J Biomol NMR* 4(6):845–858.
49. Delaglio F, et al. (1995) NMRPipe: A multidimensional spectral processing system based on UNIX pipes. *J Biomol NMR* 6(3):277–293.
50. Goddard T, Kneller D (2006) Sparky—NMR Assignment and Integration Software (University of California, San Francisco).
51. McConnell HM (1958) Reaction rates by nuclear magnetic resonance. *J Chem Phys* 28(3):430–431.
52. Strange RW, et al. (2003) The structure of holo and metal-deficient wild-type human Cu, Zn superoxide dismutase and its relevance to familial amyotrophic lateral sclerosis. *J Mol Biol* 328(4):877–891.
53. Tamiola K, Acar B, Mulder FA (2010) Sequence-specific random coil chemical shifts of intrinsically disordered proteins. *J Am Chem Soc* 132(51):18000–18003.
54. Sekhar A, Bain AD, Rumfeldt JA, Meiering EM, Kay LE (2016) Evolution of magnetization due to asymmetric dimerization: Theoretical considerations and application to aberrant oligomers formed by apoSOD1(2SH). *Phys Chem Chem Phys* 18(8):5720–5728.
55. Taylor J (1997) *Introduction to Error Analysis: The Study of Uncertainties in Physical Measurements* (University Science Books, Herndon, VA).